Planetary Nebulae: A Universal Toolbox in the Era of Precision Astrophysics
Proceedings IAU Symposium No. 384, 2025
O. De Marco, A. Zijlstra & R. Szczerba, eds.
doi:10.1017/S1743921324002011

The evolutionary path from the AGB to the PN phases: certainties and open issues

Paolo Ventura

INAF - Observatory of Rome
email: paolo.ventura@inaf.it

Abstract. The modelling of the evolutionary phases beyond the asymptotic giant branch attracts the interest of the astrophysical community because it allows the determination of the properties of progenitor stars and to deduce the efficiency of the mechanisms able to alter the surface chemistry of the stars evolving through the asymptotic giant branch. This has been possible since improvements in the modelling of these phases, which allow a reliable determination of the luminosity with which stars evolve after the termination the asymptotic giant branch evolution.

The surface chemistry of post-asymptotic giant branch stars and planetary nebulae is shown to be tightly correlated to the various processes taking place during the asymptotic giant branch evolution. The possibility of using the observed infrared excess of these evolved stars to derive information on the dust formation process during the previous evolutionary phases is also discussed.

Keywords. stars: AGB and post-AGB, stars: planetary nebulae

1. Introduction

About half century has passed since the early, pioneering attempts (Paczyński 1970a,b) to model the evolution of stars during the phases following the asymptotic giant branch (AGB), when a general contraction process begins as a reaction to the gradual ejection of the external envelope, wich precedes the white dwarf phase, not before evolving through the post-AGB and the PNe phases (Iben & Renzini 1983).

The modelling of these evolutionary phases is exceptionally difficult, owing to the combination of numerical complexities, which naturally arise along the transition from the AGB to the post-AGB, and long computational times. After the aforementioned studies, driven by Paczynski (Paczyński 1971), in which only the post-AGB phases were modelled, significant steps forward were made thanks to the studies by the Potzdam team (Bloecker & Schoenberner 1990; Bloecker 1995; Schönberner & Blöcker 1996), until the most recent investigations by Miller Bertolami (2016) and Kamath et al. (2023).

The interest towards the evolutionary phases that follow the AGB stems from the relatively easy analysis of their spectra, which allows a solid determination of the surface chemical composition (van Winckel 2003); this is at odds with AGB stars, whose spectral energy distribution is characterized by the presence of large molecular bands, which prevents a reliable estimate of the abundances of the individual chemical species (García-Hernández et al. 2006, 2009). In this regard, post-AGB and PNe sources offer notable information on the AGB phase, because their surface chemistry reflects the efficiency of the various processes able to alter the surface chemistry, primarily hot bottom burning (Renzini & Voli 1981; Bloecker & Schoenberner 1991) and third dredge-up (Iben 1974). The knowledge of the surface chemistry of the stars evolving beyond the AGB

offers a notable opportunity for their characterization: this approach was recently followed by Kamath et al. (2023), to identify a sample of Galactic post-AGB stars, and by Ventura et al. (2015, 2016, 2017); and by Stanghellini et al. (2022), to study samples of PNe in the Magellanic Clouds and in the Milky Way.

The study of post-AGB stars and PNe is also important to study dust formation in the winds of evolved stars. While significant dust formation takes place during the AGB phase (Zhukovska, Gail, & Trieloff 2008; Sloan et al. 2009), no condensation of gas molecules into solid grains is expected to occur during the very late evolutionary phases of stars. However, the dust produced during the previous AGB phases leaves a clear signature in the spectral energy distribution (SED) of post-AGB stars and PNe, in the form of a significant infrared excess. Moreover, this can be easily analysed, since the peak of the emission in the mid-IR spectral interval is clearly separated from the black-body like emission from the central stars, which peaks in the visible. In this regard, the analysis of the SED of the stars evolving through evolutionary phases beyond the AGB allows one to draw important conclusions on the dust formation rate taking place during the very late AGB phases (Tosi et al. 2022; Dell'Agli et al. 2023). Because it is during these phases that most of the dust is released, this approach opens the way towards a better comprehension of the role that AGB stars play as dust manufacturers.

In this review we will first present, in Section 2, a brief overview of the evolution of the stars through the AGB, with particular emphasis given to the role of the initial mass; in Section 3 we describe the most relevant aspects of the evolution of the stars during the phases following the AGB, along with the thermal and chemical structure; Section 4 is devoted to a historical account of the attempts to model the post-AGB phases; the importance of the study of post-AGB stars and PNe to draw information on the physical mechanisms able to alter the surface chemistry of AGB stars and as important tracers of the dust formation process during the final AGB phases are addressed, respectively, in Sections 5 and 6; the conclusions are given in the final section.

2. The evolution through the AGB: stellar structure and evolution

The evolution of the stars through the AGB is characterized by the gradual growth of the core mass, favoured by the continuous flux of H-exhausted matter into the core, connected to the CNO burning activity in a shell laying between the core and the external convective mantle (Busso, Gallino, & Wasserburg 1999; Karakas & Lattanzio 2014). The increase in core mass leads to the increase in the luminosity (Paczyński 1971), while the mass of the envelope decreases, owing to the intense mass loss experienced by these stars. The AGB evolution is also characterized by the expansion of the stellar structure. This is primarily due to the fact that the gradients of the thermodynamic variables become steeper and steeper as the AGB evolution proceeds; for carbon stars the cooling and expansion of the outer regions is further enhanced by the gradual increase in the surface carbon, which leads to the increase in the surface molecular opacities (Marigo 2002).

As far as the behaviour of the surface chemical composition is concerned, we can broadly distinguish three behaviours, related to the (initial) mass and also to the metallicity of the stars, which we describe briefly below. We note that the role of mass and metallicity are tightly connected in this context: both the minimum mass required to reach the C-star stage and the lower threshold in mass required to ignite HBB increase with metallcity (Karakas & Lattanzio 2014; Ventura et al. 2022). In what follows, we will refer to the mass of the star at the beginning of the AGB phase. These are approximately consistent with main sequence masses for $M > 1.5 M_{\odot}$; on the other hand, for lower mass stars the mass loss taking place during the red giant branch evolution must be considered, thus the masses given below must be considered as lower limit of the initial masses.

https://doi.org/10.1017/S1743921324002011 Published online by Cambridge University Press

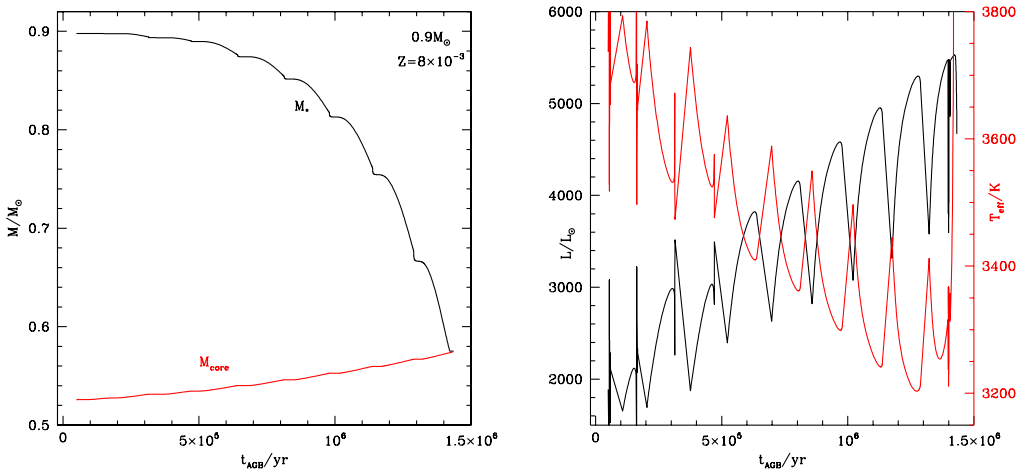

Figure 1. Left: time variation of the total mass (black line) and of the core mass (red) of a 0.9 $M_\odot$ (this mass refers to the beginning of the AGB phase, and corresponds to 1 $M_\odot$ at ZAMS) model star of metallicity $Z = 4 \times 10^{-3}$. Right: time variation of the luminosity (black line, scale on the left y-axis) and effective temperature (red, scale on the right) of the same model star.

2.1. *Low-mass stars*

The stars of mass below ~ 1 $M_\odot$ undergo a gradual loss of the external mantle, which proceeds on time scales of the order of ~ 1 Myr. An example of this kind of evolution is shown in Fig. 1, which reports the time evolution of the core and total mass of the star (left panel), and of the luminosity and effective temperature (right panel). We note the gradual rise in the luminosity, which increases from ~ 2000 $L_\odot$ to ~ 6000 $L_\odot$ during the AGB lifetime. This is accompanied by the cooling of the external regions, witnessed by the decrease in the effective temperature.

The surface chemistry of these stars is not expected to undergo significant changes during the AGB, because of the small number of thermal pulses experienced, of the order of 4-5, which prevents third dredge-up (TDU) from favouring the surface carbon enrichment. Therefore, the final chemical composition of these stars reflects the effect of the first dredge-up only (Karakas & Lattanzio 2014).

2.2. *Carbon stars*

The AGB evolution of stars of initial mass in the $1 - 3$ $M_\odot$ range is characterized by the occurrence of several TDU events, which leads to the formation of carbon stars, after the surface carbon abundance by number exceeds that of oxygen (Iben 1974).

As shown in the left panel of Fig. 2, the luminosity increases with the core mass, similarly to the low-mass counterparts discussed earlier in this section. On the other hand, we see in the right panel of the figure that repeated TDU events eventually result in the surface carbon abundance to exceed that of oxygen, which stars the carbon star phase (grey-shaded region in Fig. 2).

The achievement of the carbon star stage favours a rapid expansion of the external regions, the consequent decrease in the surface gravity, and a fast increase in the rate of mass loss (Marigo 2002; Ventura & Marigo 2009, 2010). This can be intuitively understood by looking at the behaviour of the total mass of the star in the left panel of Fig. 2, where it is clear that the rate at which the envelope is lost suddenly increases after the carbon star stage is reached. A straight consequence of this is that while the star evolves as M-type for the majority of the AGB lifetime, most of the gas ejected is carbon rich:

https://doi.org/10.1017/S1743921324002011 Published online by Cambridge University Press

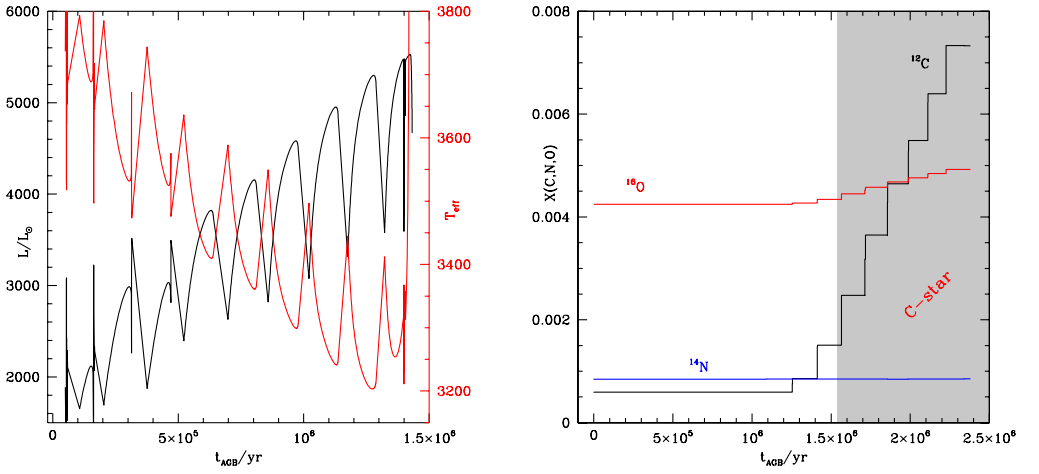

Figure 2. Left: time variation of the total and core mass (black and red lines, respectively, scale on the left y-axis) and of the luminosity (blue line, scale on the right) of a 2 $M_\odot$ model star (this is approximately the ZAMS mass, given the small mass lost by stars in this mass range during the evolutionary phases preceding the core helium burning) of metallicity $Z = 4 \times 10^{-3}$. Right: time variation of the CNO surface mass fractions of the same model star. The grey shaded area indicates the phases during which the star is a carbon star.

this is extremely important when the role of these stars as pollutants of the interstellar medium is considered.

2.3. *Massive AGB stars*

The AGB evolution of stars descending from $M > 3$ $M_\odot$ progenitors is characterized by the activation of hot bottom burning (HBB), the physical mechanism consisting in the activation of an advanced proton capture nucleosynthesis at the base of the surface envelope (Renzini & Voli 1981).

On the physical side, the activation of HBB leads to significant deviations from the core mass - luminosity relationship found by Paczyński (1971), and the luminosity of the stars, particularly of those of mass above 6 $M_\odot$, can reach 10^5 $L_\odot$ (Ventura et al. 2013). A typical example of the evolution of massive AGB stars is shown in Fig. 3, which shows the time variation of the luminosity and the temperature at the bottom of the convective envelope (top panels), and of the surface mass fractions of some chemical species (bottom panels).

We note the initial rise in the luminosity, related to the increase in the core mass, and the decline during the final AGB phases, after a significant fraction of the envelope mass was lost, which causes a general cooling of the regions of the star above the core, which gradually turn HBB off. This is confirmed by the behaviour of the temperature at the bottom of the external envelope (see top, right panel of Fig. 3), which also exhibits a decreasing trend in the second part of the AGB phase, after reaching a peak value, at an intermediate stage.

In the bottom-left panel of Fig. 3 we recognize the effects of CNO cycling, with the depletion of the surface carbon, the synthesis of nitrogen, and the reduction of the surface oxygen. We also show the behaviour of lithium, which is produced during the initial part of the AGB evolution, shortly after the ignition of HBB, owing to the activation of the Cameron & Fowler (1971) mechanism.

The bottom-right panel of Fig. 3 shows the time variation of other chemical species, from which we deduce the activation of the Ne-Na nucleosynthesis (the surface sodium

https://doi.org/10.1017/S1743921324002011 Published online by Cambridge University Press

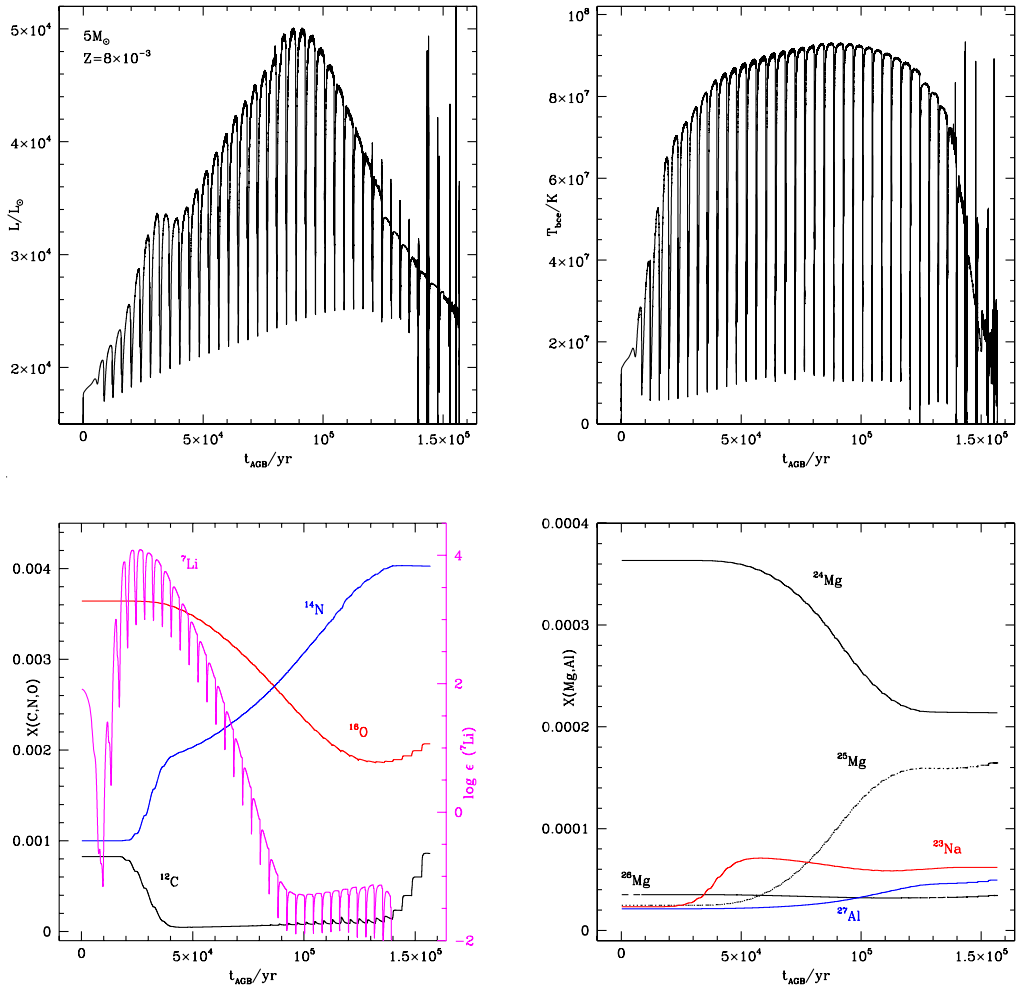

Figure 3. Top row: time variation of the luminosity (left) and temperature at the base of the convective envelope (right) of a 5 $M_\odot$ model star of metallicity $Z = 4 \times 10^{-3}$. Bottom: time variation of the surface mass fractions of lithium and of the CNO species (left), and of those involved in the Ne-Na and Mg-Al nucleosynthesis.

rises by a factor ~ 4 during the AGB phase), and of the Mg-Al chain, witnessed by the decrease in the surface ^{24}Mg and the ^{27}Al increase. The strength of the advanced p-capture nucleosynthesis associated to the ignition of HBB is extremely sensitively to the metallicity of the star (Dell'Agli et al. 2018a).

3. Post-AGB phases: stellar structure and evolution

Once the mass of the envelope of AGB stars drops below a few percents of the core mass, a contraction process begins, so that the evolutionary track moves initially to the blue, at constant luminosity (Iben & Renzini 1983). An example of such a track is shown in Fig. 4, which refers to the descendant of a 2 $M_\odot$ star of metallicity Z = 0.004, typical of the stars in the Small Magellanic Cloud (SMC) (Harris & Zaritsky 2004).

The structure of these stars, once they begin the contraction to the blue, is shown in Fig. 5, where the thermodynamic stratification in the pressure vs temperature plane is shown. In the left panel of the figure we can easily recognize: a) the core, composed by

https://doi.org/10.1017/S1743921324002011 Published online by Cambridge University Press

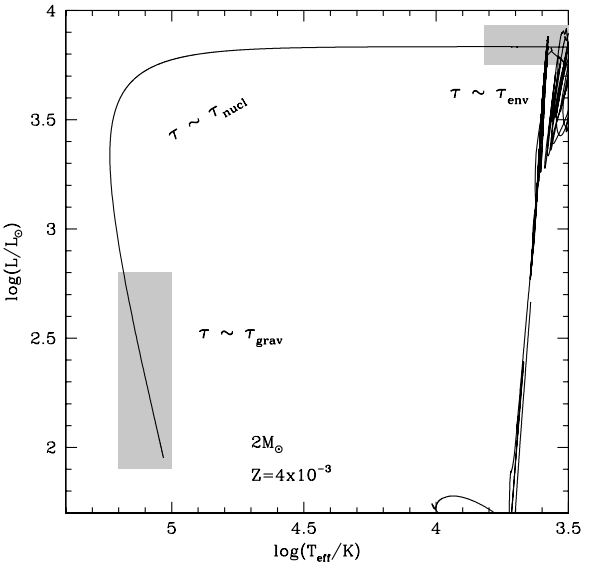

Figure 4. Evolutionary track on the HR diagram of a 2 $M_\odot$ model star of metallicity $Z = 4 \times 10^{-3}$, evolved from the start of core helium burning to the white dwarf cooling sequence. The evolutionary time scales characterizing the different parts of the track are indicated. The grey boxes in the upper and lower part of the plane indicate the parts of the evolution during which the time scale is mainly determined by the rate of mass loss and by the release of gravo-thermal energy, respectively.

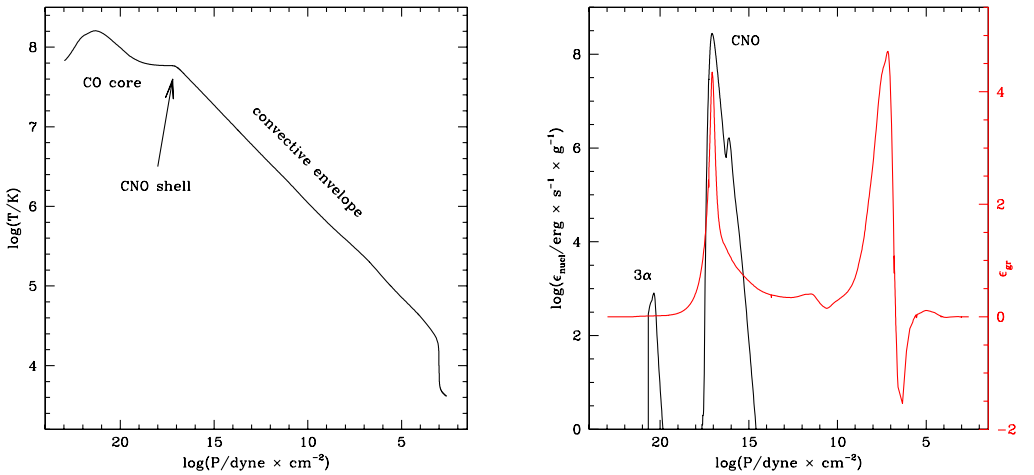

Figure 5. Left: thermodynamic structure of a 2 $M_\odot$ model star of metallicity $Z = 4 \times 10^{-3}$ during the post-AGB phase, in the pressure vs temperature plane. Right: the nuclear (black line) and gravothermal (red) coefficients for the energy release for the same structure reported in the left panel.

carbon and oxygen, supported by the pressure of degenerate electrons, which is almost isothermal; b) the CNO burning shell, located in the region where the decline of the temperature towards the outer regions of the star begins; c) the tenuous and expanded envelope, of mass ~ 0.003 $M_\odot$, which extends across more that 10 orders of magnitude in pressure. The right panel of Fig. 5 shows the gravitational and nuclear contributions to the overall energy release: we deduce that during these evolutionary phases most of the energy is related to CNO activity, with smaller contribution from gravitational

https://doi.org/10.1017/S1743921324002011 Published online by Cambridge University Press

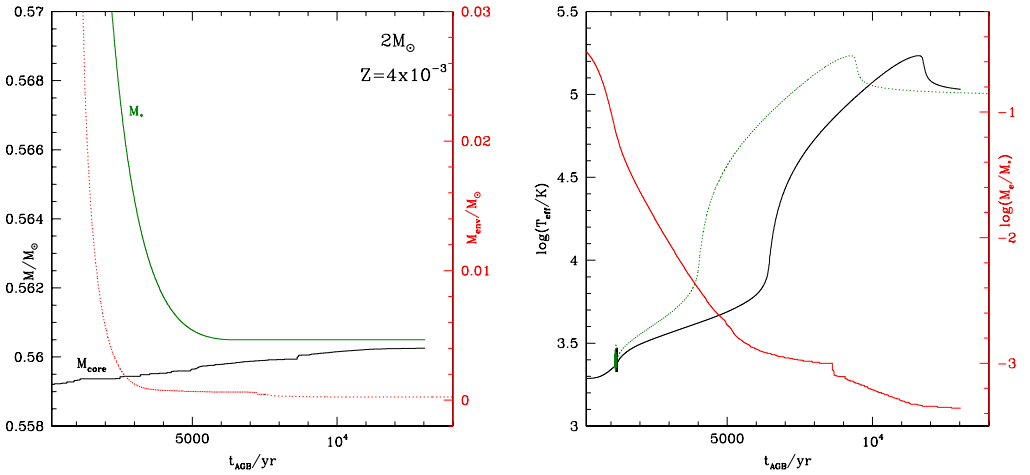

Figure 6. Left: time variation (counted from the tip of the AGB) of the core and total mass (black and green lines, respectively, scale on the left y-axis), and the mass of envelope (red, scale on the right) of the 2 $M_\odot$ model star of metallicity $Z = 4 \times 10^{-3}$ shown in Fig. 4 and Fig. 5. Right: time variation of the effective temperature (black line, scale on the left) and of the fraction of stellar mass stored in the envelope (red, scale on the right) of the same model star shown in the left panel. The green, dashed track shows the run of the effective temperature of a model star obtained by artificially enhancing, by a factor 2, the mass loss rate during the evolutionary phases following the TAGB.

contraction and negligible release from helium burning nucleosynthesis active in a more internal region of the star.

The time scale of the contraction phase is governed by different processes, related to the change in the physical conditions of the star. To discuss this point we report in the left panel of Fig. 6 the time variation of the core and total mass of the star (scale on the left vertical axis) and of the mass stored in the envelope (scale on the right), of the same model star shown in Fig. 4 and Fig. 5. The right panel of the same figure shows the evolution of the effective temperature and of the mass fraction stored in the envelope.

During the first part of the post-AGB phase the evolutionary time scale is given by the rate at which the envelope is consumed: indeed, as is clear on the left side of the left panel of Fig. 6, the run of the total and envelope mass are almost parallel during the initial post-AGB phases. This is confirmed by the results reported on the right panel of the same figure, where we show that an artificial increase in the mass-loss rate (green line) favours a faster increase in the effective temperature.

After the mass stored in the envelope drops below a few thousands of the total mass, the nuclear time scale takes over, thus the rate of contraction is mostly driven by the rate with which the core mass of the star increases, owing to the effect of the CNO nuclear activity. This is once more confirmed by the results reported in the right panel of Fig. 6, where we see that the rate at which the effective temperature increases is independent of the assumed mass-loss rate, thus indicating that the rate with which the envelope is consumed is not relevant during these evolutionary phases.

Once the mass of the envelope drops below a given threshold (which depends on the core mass and the metallicity), the CNO activity is no longer capable to supply to the star the required energy budget, thus the release of gravitational energy takes over, as the dominant energy channel. This can be see in Fig. 7, where the time variation of the various energy channels are reported. We see that the overall luminosity is essentially given by the release of nuclear energy from CNO activity until $\sim 12\,000$ yr after the

https://doi.org/10.1017/S1743921324002011 Published online by Cambridge University Press

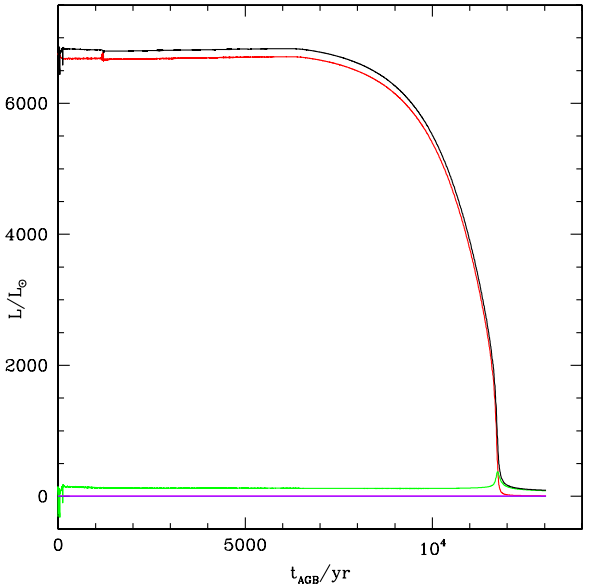

Figure 7. Time post-AGB variation of the total luminosity (black line) and of the contributions due to CNO cycling (red), 3 α reactions (magenta), gravothermal energy release (green) of the same 2 $M_{\odot}$ model star reported in the previous figures.

tip of the AGB (TAGB), and by the release of gravitational energy after that epoch. This also affects the evolutionary time-scale, which is driven by the rate with which the gravitational energy is released.

In summary, we can broadly distinguish three distinct phases characterizing the post-AGB evolution: i) the initial contraction from the tip of the AGB to the post-AGB, where the physical mechanism driving the evolution is the loss of the external envelope of the star; ii) the phase from the post-AGB, through the PNe stage, until the highest effective temperature is reached, driven by the CNO burning nuclear activity; iii) the final part of the post-AGB evolution, leading to the WD cooling sequence, when the main actor is the release of gravitational energy.

The three phases listed in the points from (i) to (iii) above are outlined in Fig. 4. We note that on the side of the duration of these phases, the first is by far the most uncertain, as it is strongly sensitive to the mass loss modelling.

4. The modelling of post-AGB phases: a historical perspective

The first attempt to model the evolutionary phases following the AGB dates back to the pioneering investigation by Paczyński (1971), who built model stars composed of a degenerate core, made up of carbon and oxygen, of mass M_c, and an outer envelope, of mass M_{env}. These studies first showed the existence of the well known relationship relating the core mass and the luminosity of the stars during the advanced, post helium-burning evolutionary phases.

In these early explorations the envelope was assumed to be static, so that the mass of the envelope was allowed to decrease gradually, and the position on the HR diagram was determined via integration of the stellar structure equations, applied to model stars characterized by the (M_c, M_{env}) combination. These studies of the post-AGB evolution demonstrated that when the mass within the envelope decreases to below $\sim 1\%$ of the total mass the evolutionary tracks move to the blue, owing to the beginning of the contraction process, which leads to hotter and hotter effective temperatures. The stage

https://doi.org/10.1017/S1743921324002011 Published online by Cambridge University Press

when the bluewards excursion of the track begins is senstitive to the core mass: the higher the core mass, the lower the fractional mass of the envelope below which the contraction process begins (Paczyński 1971).

The path traced by the evolutionary tracks on the HR diagram occurs at constant luminosity, until the CNO nuclear channel is able to provide the required energy supply, then continues towards lower luminosities, along constant radius lines, when the release of gravitational energy takes over.

A significant step forward in the modelling of the evolutionary phases following the AGB was taken by Schoenberner (1979), who calculated for the first time evolutionary sequences extended to the post-AGB and the PN phases, based on the full, self-consistent integration of the stellar structure equations, including the modelling of mass loss from the surface regions of the star. The analysis by Schoenberner (1979) was focused on two model stars descending from 1 $M_{\odot}$ and 1.45 $M_{\odot}$ progenitors.

The studies by the Potzdam group were of paramount importance to outline the role played by mass loss modelling on the results obtained, particularly for what pertains the transition time from the AGB to the post-AGB phase. A further important result regarding the evolutionary properties of these phases is the fact that the fading time scale characterizing the transition from the horizontal part of the track to the cooling sequence is given by the rate with which the gravitational energy stored into the star is dissipated (Bloecker & Schoenberner 1990): this highlights the need for a self-consistent calculation of the whole evolution through the AGB phase, in order to determine the gravitational energy reservoir of the star when contraction begins.

A more recent study on the evolutionary phases beyond the AGB was published by Miller Bertolami (2016), who presented tracks and isochrones of $0.8 - 4$ $M_{\odot}$ stars with metallicity in the $10^{-4} \leq Z \leq 2 \times 10^{-2}$ range. The times required for the star to move from the tip of the AGB to the post-AGB and the PN phase in the Miller Bertolami (2016) compilation are significantly shorter than in the models by Bloecker & Schoenberner (1990) and Vassiliadis & Wood (1994): this can be explained by the difference in the final mass versus luminosity relationship, due to the difference in the input physics and the more detailed treatment of the convective boundaries and the TDU phenomenon used. Regarding the latter point, the results reported in the recent work focused on the description of the AGB and post-AGB phases by Kamath et al. (2023) are in good agreement with those by Miller Bertolami (2016).

5. Post-AGB stars and PNe as tracers of AGB evolution

As discussed earlier in this contribution, the AGB evolution is characterized by the action of different mechanisms able to alter the surface chemical composition, primarily TDU and HBB, whose comprehension is of paramount importance to assess the role played by low and intermediate mass stars as pollutants of the interstellar medium.

On this side the analysis of the chemical composition of post-AGB stars and PNe may offer notable information on the efficiency of these processes, as it reflects the chemistry with which the stars leave the AGB, thus the results of the cumulated action of HBB and TDU over the whole AGB lifetime.

This is the approach used by Ventura et al. (2015, 2016, 2017) to investigate the PN populations of the Magellanic Clouds and of the Milky Way. These works characterized the individual sources observed in terms of mass, formation epoch and metallicity of the progenitors, based on the derived surface chemistry, which, in turn, reflects the efficiency of the aforementioned physical mechanisms.

An example of the approach followed is seen in Fig. 8, which shows the position of individual Galactic PNe studied by Ventura et al. (2017) in the (surface) C vs N plane, compared with the model predictions, found via AGB modelling. This plane was shown

https://doi.org/10.1017/S1743921324002011 Published online by Cambridge University Press

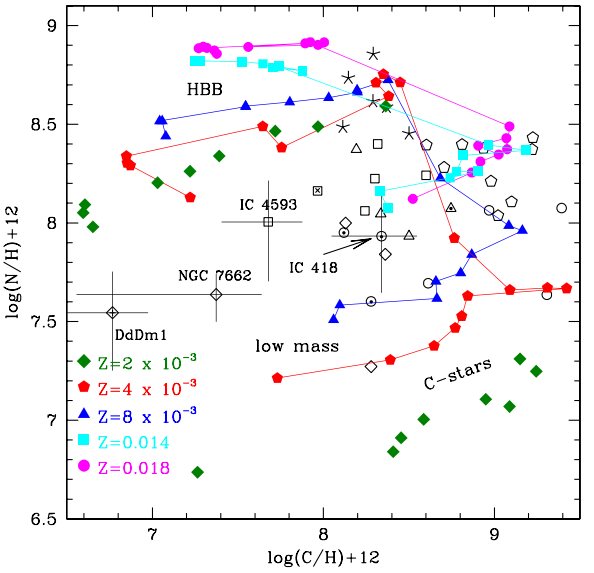

Figure 8. The final surface abundances of carbon and nitrogen of AGB models of different mass, indicated with different symbols, according to the metallicity, in the $2 \times 10^{-3} - 0.018$ range. Black symbols refer to the sample of Galactic PNe discussed in Ventura et al. (2017), for which the surface carbon is available. The different symbols correspond to the characterization of the individual sources and in particular their progenitors: open squares - descend from low-mass, solar metallicity star, which failed to reach the C-star stage; open diamonds - low-mass stars of sub-solar metallicity; open pentagons and circles: carbon stars of solar and sub-solar metallicity, respectively; open traingles and asteriscks: the progeny of stars that experienced HBB of solar and sub-solar metallicity, respectively. Dots inside symbols indicate PNe with evidence of carbon dust, whereas crosses refer to PNe with evidence of silicates. The regions of the plane where low-mass stars, C-stars and the progeny of massive AGBs that experienced HBB are indicated.

to allow the most exhaustive analysis, as stars descending from progenitors of different mass populate specific regions of the plane, according to the efficiency of the two main mechanisms responsible for the alteration of the surface chemistry. In particular, as indicated in Fig. 8, this method allows the identification of the three groups of stars discusses in Section 2: low-mass stars, carbon stars, and the progeny of massive AGBs, which experienced the HBB, easily recognized in the significant increase in the surface N.

This analysis outlined the importance of the knowledge of surface carbon, as indeed carbon is, among the different chemicals, the most sensitive to the efficiency of HBB and TDU, which cause opposite effects on the surface carbon content. The availability of the surface carbon allowed Stanghellini et al. (2022) to characterize a wide sample of Galactic PNe.

A similar approach was used by Kamath et al. (2023) to study a sample of Galactic post-AGB stars, for which the intrinsic luminosities were derived by the measured bolometric flux, benefiting from knowledge of the distances measured by Gaia. In agreement with the investigations on the PN samples of the Magellanic Clouds and the Milky Way presented by L. Stanghellini and collaborators, discussed earlier, Kamath et al. (2023) highlighted the crucial role played by the knowledge of the surface carbon as indicator of the efficiency of TDU and HBB experienced by the stars during the AGB phase. The analysis by Kamath et al. (2023) was mostly developed by studying the position of the sources considered in the surface carbon vs luminosity plane, which was shown to

https://doi.org/10.1017/S1743921324002011 Published online by Cambridge University Press

allow the most complete and reliable characterization of the individual stars considered in terms of mass, metallicity and formation epoch of the progenitors.

6. Dust around evolved stars: the new frontier

It is generally recognized that the circumstellar envelope of cool stars prove extremely favourable environment for the formation of dust, via condensation of gaseous molecules into solid particles. Among others, the dust species forming in largest quantities, thus providing the largest contribution to the overall reddening of the SED and to the acceleration of the wind via radiation pressure, are silicates, solid carbon, silicon carbide (SiC), alumina dust and solid iron (Ferrarotti & Gail 2006).

The mineralogy of the dust formed is sensitive to the surface chemistry, owing to the stability of the CO molecule, which absorbs the least abundant between carbon and oxygen in its entirety. Therefore, in C-rich environment the dust is composed of solid carbon, SiC and solid iron, whereas the winds of M-type stars, which have O-rich environments, are characterized by the formation of silicates, alumina dust and solid iron (Ferrarotti & Gail 2001, 2002, 2006).

6.1. *Dust formation modelling*

To adress the topic of dust formation in the surroundings of evolved stars some stellar evolution codes have been implemented with the schematization to model dust formation set up by the Heidelberg team (Ferrarotti & Gail 2006). In particular, Ventura et al. (2012, 2014) applied the Heidelberg method to the ATON code (Mazzitelli 1979; Ventura et al. 1998), whereas Nanni et al. (2013, 2014) coupled the same formalism to the evolutionary models calculated by means of the Colibri code (Marigo et al. 2013).

An interesting application of the combination of stellar evolution and dust formation modelling was proposed by Dell'Agli et al. (2014, 2015), to characterize the whole AGB population of the Magellanic Clouds. Later applications to this approach regarded IC 1613 (Dell'Agli et al. 2016), IC 10 (Dell'Agli et al. 2018b) and Sextans A (Dell'Agli et al. 2019). These studies will be of paramount importance now that we have entered the JWST era, which opened the way to test and extend this approach to many more galaxies in the Local Group.

6.2. *Understanding the infrared excess in the SED of post-AGB stars and PNe*

Once the AGB evolution is finished, dust formation stops, because the stars contract, the external temperature increase, thus the environmental conditions become less and less favourable to allow the condensation of gas molecules into dust. This is not the end of the story though, as the dust released until the end of the AGB leaves a distinct feature in the SED of the stars, identified as a clear IR excess. Indeed the dust moves away from the surface of the star after dust formation stops, but the dust layer is still sufficiently close to the star to leave some observational signatures, while the stars evolve through the post-AGB and the PN phases.

In this regard, Tosi et al. (2022) have recently proposed a novel approach, which allows one to use the SED of dusty post-AGB stars, to reconstruct the modality of the transition from the late AGB to the post-AGB phases, to deduce the rate of dust production during the very late AGB phases and to draw information on the dynamics of the wind, as it moves away from the star after dust formation stops. The method proposed by Tosi et al. (2022) will be of paramount importance to understanding the dust budget expected from low and intermediate mass stars during their life, as it was demonstrated that most of the

https://doi.org/10.1017/S1743921324002011 Published online by Cambridge University Press

dust released by these stars is produced during the final AGB phases, when the mass-loss rate is highest (Dell'Agli et al. 2014, 2015).

The analysis by Tosi et al. (2022) benefits from the spectral properties of post-AGB stars, particularly from the fact that the IR excess due to dust is well separated from the emission from the central star, thus the two contributions can be easily disentangled. Following Tosi et al. (2022), we find that the detailed inspection of the SED of post-AGB stars allows one to deduce the following quantities: a) the infrared optical depth, based on the relative height of the peak in the mid-IR, related to dust, compared to the main peak, related to the photospheric emission; b) the dust temperature, by the depth of the minimum in the SED separating the two peaks; c) the bolometric flux from the star, by fitting the near-IR part of the SED; d) the dust mineralogy, by examining the shape of the SED in the mid-IR wavelength region.

Point (c) proves crucial for the characterization of the individual sources considered, given the tight correlation between core mass and luminosity of these objects, discussed in Section 3. Points (a) and (b) above provide important information on the dust production rate during the very late AGB phases, as Tosi et al. (2022) demonstrated the relationship between the optical depth characterizing the star today, and that of the epoch when dust formation stopped.

This method was successfully applied by Tosi et al. (2022), to study the sample of SMC and LMC stars investigated by Kamath et al. (2014) and Kamath et al. (2015), which were classified as single stars, based on their radial velocities. Further application of this scheme was used by Dell'Agli et al. (2023) and Tosi et al. (2023) to investigate and characterize the post-AGB stars in the Milky Way presented in Kamath et al. (2022).

7. Conclusions

Progresses in stellar structure modelling allows robust modelling of the stars evolving past the AGB phase towards the white dwarf cooling sequence. This is now possible thanks to the pioneering investigations on this subject, presented over half century ago. It is now well established that these sources are mainly supported by proton-capture nucleosynthesis taking place in a H-rich shell, and that when the mass of the envelope drops below a few 10^{-3} $M_{\odot}$ the nuclear activity gradually ceases, and the release of gravothermal energy becomes the dominant energy source.

The evolutionary time scale of the post-AGB phases are first given by the speed with which the envelope is consumed, then by growth rate of the H-free core. The first is made uncertain by the poor knowledge of the mass-loss mechanism, whereas the second time scale is more robust, as it is related to the efficiency of the nuclear activity.

The synergy between the modelling of the post-AGB phases and the results from high-resolution spectroscopy of post-AGB stars and PNe allows a reliable classification of the sources investigated, in terms of mass and formation epoch of the progenitors. Furthermore, these investigations offer notable information on the previous AGB phase, as the chemical composition of post-AGB stars and PNe is the outcome of the balance between the action of TDU and HBB in modifying the surface chemical composition of the stars.

The latest research in this field have also outlined the possibility of using the SED of post-AGB stars and PN sources to infer the properties of the dust currently surrounding these stars, and to deduce the efficiency of the dust formation process during the very late AGB phases. This method proves highly effective to evaluate the role of AGB stars as dust manufactures, considering that most of the dust is produced during the late AGB phases.

https://doi.org/10.1017/S1743921324002011 Published online by Cambridge University Press

Acknowledgements

The author acknowledges support from the National Institute for Astrophysics (INAF) within the theory grant *Understanding mass loss and dust production from evolved stars* (Ob. 1.05.12.06.07, PI. P. Ventura) and the PRIN 2019 grant *Building up the halo: chemodynamical tagging in the age of large surveys* (Ob. 1.05.01.85.14, PI. S. Lucatello)

References

Blöecker, T., Schöenberner, D. 1990, *A&A*, 240, L11
Blöecker, T., Schöenberner, D. 1991, *A&A*, 244, L43
Blöecker, T. 1995, *A&A*, 299, 755
Busso, M., Gallino, R., Wasserburg, G. J. 1999, *ARA&A*, 37, 239
Cameron, A. G. W., Fowler, W. A. 1971, *ApJ*, 164, 111
Dell'Agli, F., Ventura, P., García-Hernández, D. A., Schneider, R., Di Criscienzo, M., Brocato, E., D'Antona, F., et al. 2014, *MNRAS*, 442, L38
Dell'Agli, F., Ventura, P., Schneider, R., Di Criscienzo, M., García-Hernández, D. A., Rossi, C., Brocato, E. 2015, *MNRAS*, 447, 2992
Dell'Agli, F., Di Criscienzo, M., Boyer, M. L., García-Hernández, D. A. 2016, *MNRAS*, 460, 4230
Dell'Agli, F., García-Hernández, D. A., Ventura, P., Mészáros, S., Masseron, T., Fernández-Trincado, J. G., Tang, B., et al. 2018a, *MNRAS*, 475, 3098
Dell'Agli, F., Di Criscienzo, M., Ventura, P., Limongi, M., García-Hernández, D. A., Marini, E., Rossi, C. 2018b, *MNRAS*, 479, 5035
Dell'Agli, F., Di Criscienzo, M., García-Hernández, D. A., Ventura, P., Limongi, M., Marini, E., Jones, O. C. 2019, *MNRAS*, 482, 4733
Dell'Agli, F., Tosi, S., Kamath, D., Stanghellini, L., Bianchi, S., Ventura, P., Marini, E., et al. 2023, *MNRAS*, 526, 5386
Ferrarotti, A. S., Gail, H.-P. 2001, *A&A*, 371, 133
Ferrarotti, A. S., Gail, H.-P. 2002, *A&A*, 382, 256
Ferrarotti, A. S., Gail, H.-P. 2006, *A&A*, 447, 553
García-Hernández, D. A., García-Lario, P., Plez, B., D'Antona, F., Manchado, A., Trigo-Rodríguez, J. M., 2006, *Sci*, 314, 1751
García-Hernández, D. A., Manchado, A., Lambert, D. L., Plez, B., García-Lario, P., D'Antona, F., Lugaro, M., et al. 2009, *ApJL*, 705, L31
Harris, J., Zaritsky, D. 2004, *AJ*, 127, 1531
Iben, I. 1974, *ARA&A*, 12, 215
Iben, I., Renzini, A. 1983, *ARA&A*, 21, 271
Kamath, D., Wood, P. R., Van Winckel, H. 2014, *MNRAS*, 439, 2211
Kamath, D., Wood, P. R., Van Winckel, H. 2015, *MNRAS*, 454, 1468
Kamath, D., Van Winckel, H., Ventura, P., Mohorian, M., Hrivnak, B. J., Dell'Agli, F., Karakas, A. 2022, *ApJL*, 927, L13
Kamath, D., Dell'Agli, F., Ventura, P., Van Winckel, H., Tosi, S., Karakas, A. I. 2023, *MNRAS*, 519, 2169
Karakas, A. I., Lattanzio, J. C. 2014, *PASA*, 31, e030
Marigo, P. 2002, *A&A*, 387, 507
Marigo, P., Bressan, A., Nanni, A., Girardi, L., Pumo, M. L. 2013, *MNRAS*, 434, 488
Mazzitelli, I. 1979, *A&A*, 79, 251
Miller Bertolami, M. M. 2016, *A&A*, 588, A25
Nanni, A., Bressan, A., Marigo, P., Girardi, L. 2013, *MNRAS*, 434, 2390
Nanni, A., Bressan, A., Marigo, P., Girardi, L. 2013, *MNRAS*, 438, 2328
Paczyński, B. 1970a, *AcA*, 20, 47
Paczyński, B. 1970, *AcA*, 20, 287
Paczyński, B. 1971, *AcA*, 21, 417
Renzini, A., Voli, M. 1981, *A&A*, 94, 175

Schöenberner, D. 1979, *A&A*, 79, 108
Schönberner, D., Blöcker, T. 1996, *Ap&SS*, 245, 201
Sloan, G. C., Matsuur,a M., Zijlstra, A. A., Lagadec, E., Groenewegen, M. A. T., Wood, P. R., Szyszka, C., et al. 2009, *Sci*, 323, 353
Stanghellini, L., Bushra, R., Shaw, R. A., Dell'Agli, F., García-Hernández, D. A., Ventura, P. 2022, *ApJ*, 929, 148
Tosi, S., Dell'Agli, F., Kamath, D., Ventura, P., Van Winckel, H., Marini, E. 2022, *A&A*, 668, A22
Tosi, S., Kamath, D., Dell'Agli, F., Van Winckel, H., Ventura, P., Marchetti, T., Marini, E., et al. 2023, *A&A*, 673, A41
van Winckel, H. 2003, *ARA&A*, 41, 391
Vassiliadis, E., Wood, P. R. 1994, ApJS, 92, 125
Ventura, P., Zeppieri, A., Mazzitelli, I., D'Antona, F. 1998, *A&A*, 334, 953
Ventura, P., Marigo, P. 2009, *MNRAS*, 399, L54
Ventura, P., Marigo, P. 2010, *MNRAS*, 408, 2476
Ventura, P., Di Criscienzo, M., Schneider, R., Carini, R., Valiante, R., D'Antona, F., Gallerani, S., et al. 2012, *MNRAS*, 424, 2345
Ventura, P., Di Criscienzo, M., Carini, R., D'Antona, F. 2013, *MNRAS*, 431, 3642
Ventura, P., Dell'Agli, F., Schneider, R., Di Criscienzo, M., Rossi, C., La Franca, F., Gallerani, S., et al. 2014, *MNRAS*, 439, 977
Ventura, P., Stanghellini, L., Dell'Agli, F., García-Hernández, D. A., Di Criscienzo, M. 2015, *MNRAS*, 452, 3679
Ventura, P., Stanghellini, L., Di Criscienzo, M., García-Hernández, D. A., Dell'Agli, F. 2016, *MNRAS*, 460, 3940
Ventura, P., Stanghellini, L., Dell'Agli, F., García-Hernández, D. A. 2017, *MNRAS*, 471, 464
Ventura, P., Dell'Agli, F., Tailo, M., Castellani, M., Marini, E., Tosi, S., Di Criscienzo, M., 2022, *Univ*, 8, 45
Zhukovska, S., Gail, H.-P., Trieloff, M. 2008, *A&A*, 479, 453

https://doi.org/10.1017/S1743921324002011 Published online by Cambridge University Press